29th Congress of the International Council
of the Aeronautical Sciences
St. Petersburg, Russia; September 7~12, 2014

EVALUATIONS OF FLYING QUALITIES FOR A NEW AND AN AGING TRANSPORT AIRCRAFT IN SEVERE ATMOSPHERIC TURBULENCE

Ray C. Chang *, C. Edward Lan**, Wen-Lin Guan***

* Dept. of Aviation Mechanical Engineering, China University of Science and Technology, Taiwan, R.O.C
** Dept, of Aerospace Engineering, University of Kansas, Lawrence, Kansas, 66045,
USA *** Investigation Laboratory, Aviation Safety Council, Taipei, Taiwan, R.O.C

Abstract

The transport aircraft response to atmospheric turbulence has been of great concern in recent years among all kinds of adverse weather conditions. The main focus is the sudden plunging motion with the abrupt change in altitude because it affects the flight safety the most in severe atmospheric turbulence. The main objective of this paper is to present a comparative analysis of flying qualities for a new and an aging twin-jet transports by using the eigenvalues of flight motion modes for transport aircraft in severe atmospheric turbulence with sudden plunging motion in transonic flight. These two similar twin-jet transports are employed for comparative analysis. The longitudinal and lateral-directional motion modes are analyzed through digital flight simulation based on decoupled dynamic equations of motion. The eigenvalue equations of the decoupled dynamic equations of motion are polynomials of the 4th degree and their roots are solved with a quadratic factoring method based on the Lin-Bairstow algorithm. It is shown that the magnitude of the imaginary part of eigenvalues can be related to the severity of plunging motion and can be used as a key parameter in describing the level of load factor it will reach. A low value of the imaginary part implies low system stiffness. A low load factor reached in plunging motion should affect flight safety the most.

1 Introduction

Among the different types of atmospheric disturbances, atmospheric turbulence has been an important cause affecting flight safety. The atmospheric turbulence severity had been estimated in real time from in-situ aircraft measurements [1]. The purpose was to estimate the eddy dissipation rate from the measurement of aircraft normal acceleration based on the assumption of a homogeneous, continuous, linear von Kármán turbulence model coupled with a linear transfer function of the aircraft dynamics. This model of National Center of Atmospheric Research (NCAR) was intended for continuous turbulence environment. Therefore, this method could not handle the type of cases involving gust with sudden plunging motion.

In refer. [2], a technique of a normal-force in-situ turbulence algorithm for aircraft was toward skipping the measurement of turbulence itself (i.e., eddy dissipation rate) and directly reporting (or deriving) the aircraft response (hazard) instead, still based on steady linear aerodynamics. The turbulence hazard is quantified in terms of the root-mean-square (RMS) normal loads over a moving 5-second interval to define the severity of turbulence in refer. [3]. The correlation coefficient of the RMS normal loads to the peak loads is determined to be 0.89 in 102 cases. The estimation was based on the assumption of continuous turbulence. However, experience indicates that most flight injuries in atmospheric turbulence have been caused by sudden plunging motion with a localized region of strong turbulence.

Many atmospheric turbulence related occurrences of transport aircraft in Taiwan, ROC, have been reported in the past, especially on en-route turbulence over the ocean near Japan during cruise flight. The evaluations of stability characteristics during sudden plunging motion through oscillatory derivatives along the flight path for a transport aircraft encountering severe atmospheric turbulence were demonstrated in refer. [4]. The use of oscillatory derivative instead of steady damping ones was more consistent with the actual case of the aerodynamic damping in the analysis of stability characteristics in this reference.

The evaluations of flying qualities during sudden plunging motion for a twin-jet transport aircraft encountering severe atmospheric turbulence through digital 6-DOF flight simulations in transonic flight were presented in refer. [5]. To numerically integrate the 6-DOF dynamic equations of motion and determine the eigen-modes of motion at the same time at every instant were the important process of this approach. The longitudinal equations being coupled with the lateral-directional equations and some nonlinear effects being incorporated were the advantages for 6-DOF flight simulations. The eigenvalue equations were solved with QR transformation. Unfortunately, this approach was difficult to identify the individual modes of motion from these eigenvalues, from one instant, to another because of the rapid changes of aerodynamic forces and moments in turbulence.

Regarding to the evaluations of dynamic stability characteristics and flight handling quality, one approach in reference [6] to solve the problems of 6-DOF flight simulations was to use the approximate modes of motion obtained from decoupled longitudinal and lateral-directional equations. In this reference, the CAP (Control Anticipation Parameter) index and normal load factor per unit angle of attack were used to depict the degradation of the flight handling quality, but the longitudinal short-period mode was the only mode to be analyzed in this reference.

To provide the mitigation concepts and promote the understanding of aerodynamic responses, a new study to examine the effects of severe atmospheric turbulence on dynamic stability characteristics is undertaken. This paper presents fuzzy-logic modeling (FLM) technique to establish nonlinear and unsteady aerodynamic models for six aerodynamic coefficients based on the flight data of two similar twin-jet transports. The new one of these two transports encountered severe atmospheric turbulence twice during the descending phase and another aging one encountered severe atmospheric turbulence in cruise phase. The oscillatory derivatives extracted from these aerodynamic models are then used in the study of variations in flying qualities during the sudden plunging motion. The longitudinal and lateral-directional motion modes are analyzed through digital flight simulation based on decoupled dynamic equations of motion. The eigenvalue equations are formulated in the form of polynomials and solved. The eigenvalues for short-period, phugoid (long-period), Dutch roll, spiral, and roll modes of motion are estimated based on damping ratio and undamped natural frequency. A positive real part of the eigenvalues is to indicate unstable motion of the related modes. The evaluations of unstable conditions for each eigen mode with the oscillatory derivatives are demonstrated in the present paper.

2 Present Method of Analysis

2.1 Fuzzy-Logic Thrust Model
Regarding to the flight dynamic equations in refer. [7], the thrust terms are in the equations of three forces and pitching moment about the airplane body axes. For the two similar twin-jet transports in the present study, only the axial force and the pitching moment are affected by thrust. Since the examination of the stability characteristics is performed with the actual flight data, an accurate thrust model for simulation is important for the present study. The thrust model is set up to vary with proper flight variables that are available in the flight data and flight manual. A detailed description of the thrust model development is available in refer. [7].

The new and aging twin-jet transports employ GE and Pratt & Whitney turbofan engines, respectively in the present study. For

GE turbofan engines, the rpm of the low-pressure compressor (N_1) is used to set the level of thrust (T), so that the thrust model is set up as:

$$T = f(h, W, M, \text{CAS}, N_1, \dot{m}_f) \qquad (1)$$

where the variables of right hand sides in Eq. (1) represent flight altitudes (h), weights (W), Mach numbers (M), computed (or calibrated) airspeed (CAS), rpm of low-pressure compressor (N_1), and fuel flow rates ($\dot{m}_f$).

For the Pratt & Whitney engines, thrust (T) is defined by engine pressure ratios (EPR), so that the thrust model is set up as:

$$T = f(h, W, M, \text{CAS}, \text{EPR}, \dot{m}_f) \qquad (2)$$

Once the thrust models are generated as a function with the flight conditions of climbing and cruise, one can estimate the thrust magnitude by inserting these flight variables from the flight data into the model.

2.2 Fuzzy-Logic Aerodynamic Models

Modeling means to establish the numerical relationship among certain variables of interest. In the fuzzy-logic models, more complete necessary influencing flight variables can be included to capture all possible effects on aircraft response to atmospheric disturbances. For longitudinal aerodynamics, the models are assumed to be of the form:

$$C_x, C_z, C_m = f(\alpha, \dot{\alpha}, q, k_1, \beta, \delta_e, M, p, \delta_s, \overline{q}) \qquad (3)$$

The coefficients on the left hand side of Eq. (3) represent the coefficients of axial force (C_x), normal force (C_z), and pitching moment (C_m), respectively. The variables on the right hand side of Eq. (3) denote the angle of attack (α), time rate of angle of attack ($d\alpha/dt$, or $\dot{\alpha}$), pitch rate (q), longitudinal reduced frequency (k_1), sideslip angle (β), control deflection angle of elevator (δ_e), Mach number (M), roll rate (p), stabilizer angle (δ_s), and dynamic pressure ($\overline{q}$). These variables are called the influencing variables. The roll rate is included here because it is known that an aircraft encountering hazardous weather tend to develop rolling which may affect longitudinal stability. The inclusion of dynamic pressure is for estimation of the significance in structural deformation effects.

For the lateral-directional aerodynamics,

$$C_y, C_l, C_n = f(\alpha, \beta, \phi, p, r, k_2, \delta_a, \delta_r, M, \dot{\alpha}, \dot{\beta}) \qquad (4)$$

The coefficients on the left hand side of Eq. (4) represent the coefficients of side force (C_y), rolling moment (C_l) and yawing moment (C_n), respectively. The variables on the right hand side of Eq. (4) denote the angle of attack (α), sideslip angle (β), roll angle (ϕ), roll rate (p), yaw rate (r), lateral-directional reduced frequency (k_2), control deflection angle of aileron (δ_a), control deflection angle of rudder (δ_r), Mach number (M), the time rate of angle of attack ($\dot{\alpha}$), and the time rate of sideslip angle ($\dot{\beta}$).

2.3 Flight Simulation

Since the rapid changes of aerodynamic forces and moments in turbulence, it is difficult to identify the individual modes of motion from these eigenvalues through digital 6-DOF flight simulations from one instant to another. Regarding to the evaluations of flying qualities, one approach to solve this problem is to use the approximate modes of motion obtained from decoupled longitudinal and lateral-directional equations as guidance.

The decoupled linearized longitudinal equations of motion, which are decoupled from the lateral-directional motions in [8], are given by

$$\dot{u} = -g\theta\cos\theta_1 + X_u u + X_\alpha \alpha + X_{\delta e}\delta e \qquad (5)$$

$$U_1\dot{\alpha} - U_1\dot{\theta} = -g\theta\sin\theta_1 + Z_u u + Z_\alpha \alpha + \qquad (6)$$
$$Z_{\dot{\alpha}}\dot{\alpha} + Z_q\dot{\theta} + Z_{\delta e}\delta e$$

$$\ddot{\theta} = M_u u + M_\alpha \alpha + M_{\dot{\alpha}}\dot{\alpha} + M_q\dot{\theta} + M_{\delta e}\delta e \qquad (7)$$

where the X_u, X_α, and $X_{\delta e}$ are the dimensional variations of force along X axis with the speed, angle of attack, and elevator angle, respectively; the other dimensional derivatives of Z and M are described and given in [8]. The decoupled lateral-directional equations of motion are:

$$U_1\dot{\beta} + U_1\dot{\psi} = g\phi\cos\theta_1 + Y_\beta \beta + Y_p\dot{\phi} + Y_r\dot{\psi} + \qquad (8)$$
$$Y_{\delta a}\delta a + Y_{\delta r}\delta r$$

$$\ddot{\phi} - \overline{A}_1\ddot{\psi} = L_\beta \beta + L_p\dot{\phi} + L_r\dot{\psi} + L_{\delta a}\delta a + L_{\delta r}\delta r \qquad (9)$$

$$\ddot{\psi} - \overline{B}_1\ddot{\phi} = N_\beta \beta + N_p\dot{\phi} + N_r\dot{\psi} + N_{\delta a}\delta a + N_{\delta r}\delta r \qquad (10)$$

where $\overline{A}_1 = I_{xz}/I_{xx}$ and $\overline{B}_1 = I_{xz}/I_{zz}$; the dimensional derivatives of Y, L, and N are described and given in [8]. The characteristic equations for Eqs, (5)~(7), and Eqs. (8)~(10) are polynomials of the 4th degree and their roots are

solved with a quadratic factoring method based on the Lin-Bairstow algorithm in [9].

The 4th degree polynomial of longitudinal characteristic equations has 4 roots; they are two complex conjugates [8]. One of the two complex conjugates represents the short-period mode. Another one is the phugoid mode (long period mode). Each mode has the same real part, but with imaginary parts of equal magnitude and opposite signs. The 4th degree polynomial of lateral-directional characteristic equations also has 4 roots; they are one pair of complex conjugates and two real values. The pair of complex conjugates represent the Dutch roll mode. One of two real values represents the spiral mode and another one represents the roll mode.

3 Numerical Results and Discussions

3.1 Flight Data

In the present paper, two similar twin-jet transports are employed as the study case for comparative analysis. Transport A, a newer one encountered atmospheric turbulence twice during the descending phase. The first and the second atmospheric turbulence encounters were at altitude about 10342 m and 9046 m, respectively. The dataset used for the modeling are extracted from the flight data recorder (FDR) during turbulence encounter lasting for 260 seconds.

The main aircraft geometric and inertial characteristics for Transport A are taken to be:
W (take-off) = 1,767,740 N (397271 lb)
S = 361.3 m^2 (3890 ft^2), $\bar{c}$ = 6.005 m (19.7 ft),
b= 60.289 m (197.8 ft)
I_{xx} = 12,815,012 kg-m^2 (9,452,600 slugs-ft^2), I_{yy} =12,511,197 kg-m^2 (9,228,500 slugs-ft^2)
I_{zz} = 53,650,986 kg-m^2 (39,574,000 slugs-ft^2),
I_{xz} = 0.0 kg-m^2

Transport B, the aging one encountered atmospheric turbulence once during the cruise flight with airspeed of 519 km/hr (280 knots) and altitude about 10,050 m. The dataset used for the modeling are extracted from the FDR during turbulence encounter lasting for 92 seconds.

The main aircraft geometric and inertial characteristics for Transport B are taken to be:

W (take-off) = 1,431,800 N (321900 lb)
S = 260 m^2 (2798.7 ft^2), $\bar{c}$ = 6.608 m (21.68 ft),
b = 44.827 m (147.08 ft)
I_{xx} = 10,710,000 kg-m^2 (7,899,900 slugs-ft^2), I_{yy} = 14,883,800 kg-m^2 (10,978,000 slugs-ft^2)
I_{zz} = 25,283,271 kg-m^2 (18,648,470 slugs-ft^2),
I_{xz} = 0.0 kg-m^2

The necessary data in the FDR to determine the aerodynamics for transports A and B are time (t), CAS, pressure altitude (h), Euler angles (ϕ, θ, and ψ), the longitudinal, lateral, and vertical accelerations (a_x, a_y, a_z), angle of attack (α), aileron deflection (δ_a), elevator (δ_e), rudder (δ_r), stabilizer (δ_s), engine EPR, outside air temperature, wind speed, wind direction, and fuel flow rate. Since only the normal acceleration is recorded in 8-Hz resolution (i.e. 8 points per second), all other parameters are interpolated with a monotone cubic spline to the same sampling rate.

3.2 Aerodynamic and Flight Environments
Both Transports A and B encountered severe atmospheric turbulences in revenue flights. As a result, several passengers and cabin crews sustained injuries, because of which these two events were classified as the aviation accidents. To examine the flying qualities, it is imperative to understand the flight environment in detail.

The corresponding flight data for Transport A in severe atmospheric turbulence in plunging motion is presented in Fig. 1. The dataset of time span from t=7480~7739 sec used for the modeling are extracted from the FDR. As indicated earlier, Transport A encounters severe atmospheric turbulence twice during this time span. In Fig. 1(a), the variations of normal acceleration (a_z) show the highest a_z being 2.05g around t = 7483 sec and the lowest being-1.05 g around t = 7484 sec in the first turbulence encounter; while the highest a_z being 1.91g around t = 7682 sec and the lowest being -0.16 g around t = 7684 sec in the second one. Fig. 1(b) shows that variation of α is approximately in phase with a_z during those two turbulence encounters; α is highest about 4 deg. in the first turbulence encounter and 5.5 deg. in the second one. The altitude (h) with drop-off heights in the first turbulence encounter with time span from t=7482~7494 sec is presented in Fig. 1(c) and in the second turbulence encounter with time span

from t=7680~7690 sec is presented in Fig. 1(d). The aircraft rapidly plunges downward during the turbulence encounter. The largest drop-off height reaches 57.3 m in the time span between t = 7484~7486 sec, as shown in Fig. 1(c). The Mach number (M) drops from 0.83 to 0.75 in the first turbulence encounter and from 0.80 to 0.70 in the second one, as shown in Fig. 1(e).
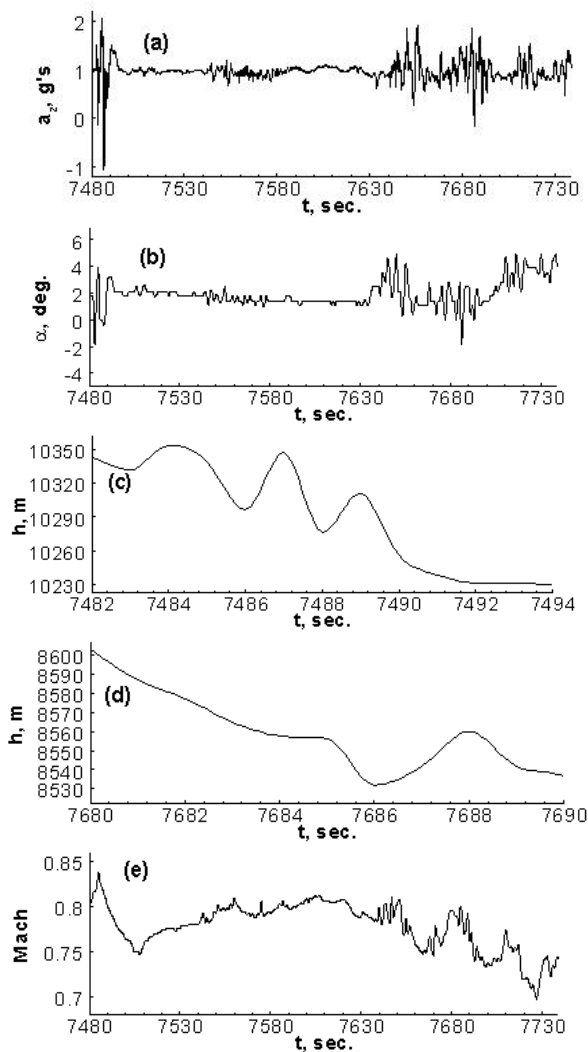

Fig. 1 Time history of flight variables for Transport A in severe atmospheric turbulence during the descending phase in transonic flight

The corresponding flight data for Transport B in severe atmospheric turbulence at the altitude around 10,050 m in transonic flight is presented in Fig. 2. The variation of normal acceleration is presented in Fig. 2(a), showing the highest a_z being 1.75 g around t = 3930 sec and the lowest being 0.02 g around t = 3932 sec.

Fig. 2(b) shows that α is approximately in phase with a_z. When a_z is the highest (around $t = 3930$ sec), the aircraft rapidly plunging downward with the drop-off height of 60 m as shown in Fig. 2(c); and α is highest about 6.5 deg. in Fig. 2(b). At the same time, M is around 0.77 in Fig. 2(d).
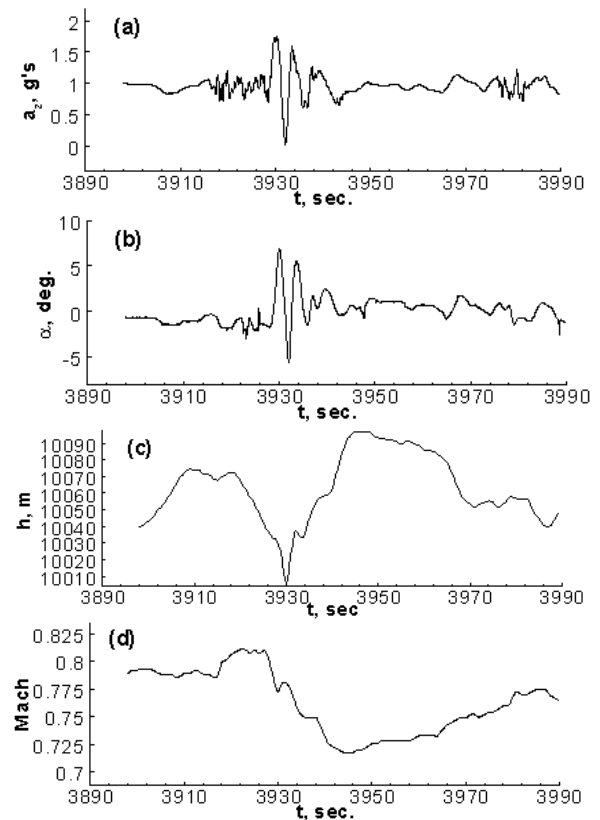

Fig. 2 Time history of flight variables for Transport B in severe atmospheric turbulence at the altitude around 10,050 m in transonic flight

The dynamic aerodynamic effects can be expected to be very significant under the circumstances of nearly instantaneous changes of α, h, and M in transonic flight. Since α of transport A and transport B reaches the value about 5.0 deg. in transonic flight, compressibility effect is important. It should be noted that the turbulent vertical wind field was not measured or estimated in the FDR; but is included in the total α. The highest a_z value of Transport A is larger than that of Transport B, but the drop-off height and angles of attack variations of Transport A are less than those of Transport B.

3.3 Analysis of Model Predictions

In the present study, the accuracy of the established unsteady aerodynamic models with six aerodynamic coefficients by using FLM technique is estimated by the sum of squared errors (SSE) and the square of multiple correlation coefficients (R^2). All the aerodynamic derivatives in the study of flying qualities are calculated with these aerodynamic models of aerodynamic coefficients.

Fig. 3 and Fig. 4 present the aerodynamic coefficients of normal force C_z, pitching moment C_m, rolling moment C_l, and yawing moment C_n predicted by the unsteady aerodynamic models of Transport A and Transport B, respectively. The predicted results by the final models have good match with the flight data. The scattering of C_m-data in Fig. 4(b) is most likely caused by turbulence-induced buffeting on the structure, in particular on the horizontal tail. Once the aerodynamic models are set up, one can calculate all necessary derivatives by central difference scheme to analyze the stability characteristics.

The final main aerodynamic models of aerodynamic coefficients consist of many fuzzy rules for each coefficient as described from Table 1 to Table 4. In Tables 1~4, the numbers below each input variable represents the number of membership function. The total number of fuzzy cells (n) in each model is the product of each number which is presented in column 3. The last column shows the final multiple correlation coefficients (R^2). The accuracy of

the established aerodynamic model through the fuzzy-logic algorithm can be judged by the multiple correlation coefficients (R^2).
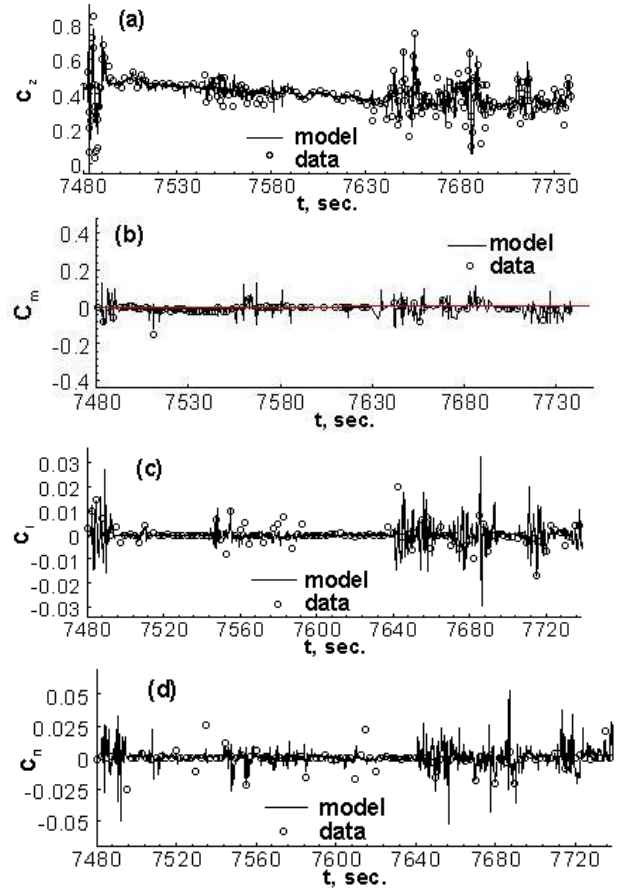

Fig. 3 Main aerodynamic coefficients predicted by the unsteady aerodynamic models of Transport A

Table 1 Final main models of longitudinal aerodynamics for Transport A

Coef.	α	$\dot{\alpha}$	q	k_1	β	δ_e	M	p	$\overline{q}$	n	R^2
C_z	2	3	3	2	3	3	2	3	2	3888	0.9618
C_m	2	2	3	4	2	3	2	2	3	3456	0.9873

Table 2 Final main models of lateral-directional aerodynamics for Transport A

Coef.	α	β	ϕ	p	r	k_2	δ_a	δ_r	M	$\dot{\alpha}$	$\dot{\beta}$	n	R^2
C_l	2	3	3	2	2	3	2	2	3	3	2	15552	0.9617
C_n	3	2	4	2	2	2	3	3	2	2	2	13824	0.9435

Table 3 Final main models of longitudinal aerodynamics for Transport B

Coef.	α	$\dot{\alpha}$	q	k_1	β	δ_e	M	p	δ_s	$\overline{q}$	n	R^2
C_z	2	4	2	2	3	2	2	2	3	2	4608	0.9789
C_m	2	2	4	2	2	4	2	2	2	2	4096	0.9579

Table 4 Final models of lateral-directional aerodynamics for Transport B

Coef.	α,	β,	ϕ,	p,	r,	k_2,	δ_a,	δ_r,	M,	$\dot{\alpha}$,	$\dot{\beta}$	n	R^2
C_l	4	2	2	4	2	3	2	2	2	2	2	12288	0.9533
C_n	2	2	2	2	4	2	2	4	2	2	2	8192	0.9435
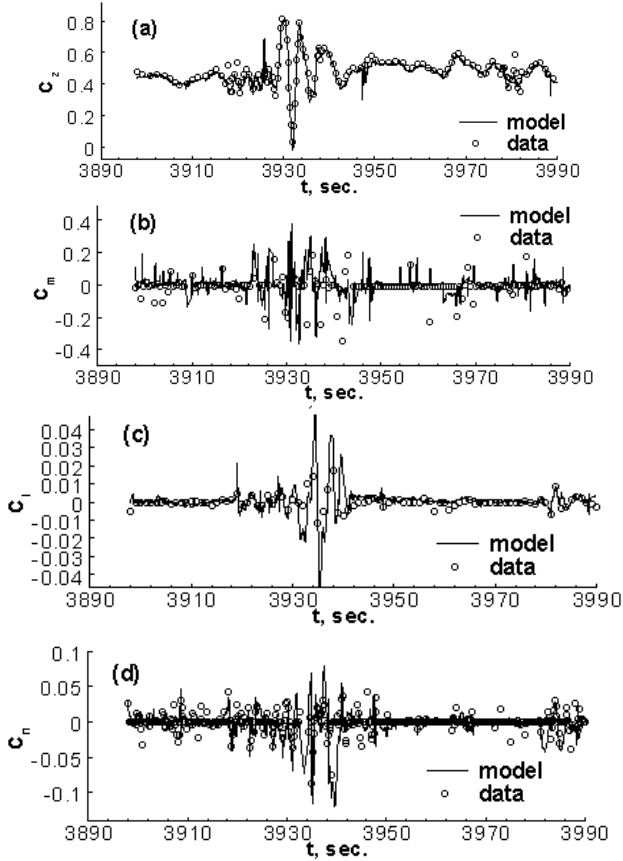
Fig. 4 Main aerodynamic coefficients predicted by the unsteady aerodynamic models of Transport B

3.4 Analysis of Stability Characteristics in Oscillatory Motion

Since the sudden plunging motion with the abrupt change in altitude affects the flight safety the most in severe atmospheric turbulence. The time periods of 7482 ~ 7494 sec and 3927.5 ~ 3932.5 sec are emphasized in evaluating the stability characteristics for Transports A and B, respectively. In order to evaluate the variations in characteristics, the units of all aerodynamic derivatives are converted to rad^{-1}. It should be noted that these derivatives are evaluated at the instantaneous conditions, instead of about the trim conditions as have been traditionally done.

Figs. 5 and 6 present the time history of main longitudinal and lateral-directional oscillatory derivatives for Transports A and B, respectively along the flight path to associate with $\dot{\alpha}$ and $\dot{\beta}$-derivatives. Note that in Fig. 5(a) and 6(a), the oscillatory derivatives are defined as:

$$(C_{mq})_{osc} = C_{mq} + C_{m\dot{\alpha}} \tag{11}$$

$$(C_{zq})_{osc} = C_{zq} + C_{z\dot{\alpha}} \tag{12}$$

In Fig. 5(c) and Fig. 6(c), the oscillatory derivatives are defined as

$$(C_{lp})_{osc} = C_{lp} + C_{l\dot{\beta}} sin\ \alpha \tag{13}$$

$$(C_{nr})_{osc} = C_{nr} - C_{n\dot{\beta}} cos\ \alpha \tag{14}$$

The values of oscillatory derivatives are equivalent to the combinations of steady damping and dynamic derivatives in above Eqs. (11) ~ (14). The use of oscillatory derivative instead of steady damping only is more consistent with the actual case of the aerodynamic steady damping in the analysis of stability characteristics. To be stable, $(C_{zq})_{osc} > 0$, $(C_{mq})_{osc} < 0$, $(C_{lp})_{osc} < 0$, and $(C_{nr})_{osc} < 0$. Physically, if it is unstable, the motion could be divergent in oscillatory motions within a short time period. The values in the period of plunging motion have some differences between oscillatory and steady damping derivatives in Figs 5(a) and 5(c) for Transport A due to the effects of the dynamic derivatives (i.e. $\dot{\alpha}$ and $\dot{\beta}$-derivatives), so as Figs 6(a) and 6(c) for Transport B.
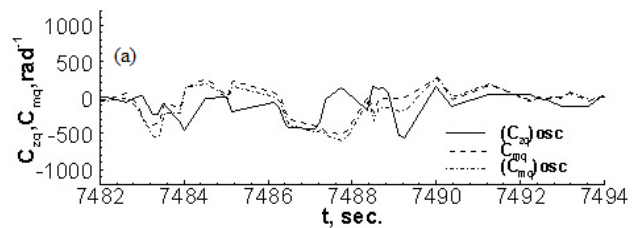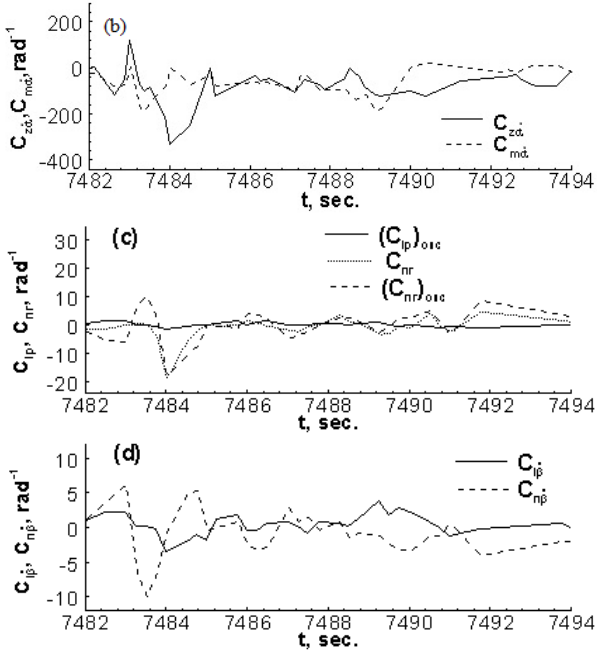
Fig. 5 Time history of main longitudinal and lateral-directional oscillatory derivatives along the flight path

Figs 5(b) and 5(d) show dynamic derivatives of stability for Transport A. To be stable, $C_{z\dot{\alpha}} > 0$, $C_{m\dot{\alpha}} < 0$, $C_{l\dot{\beta}} < 0$, and $C_{n\dot{\beta}} > 0$. The magnitudes of $C_{z\dot{\alpha}}$ and $C_{m\dot{\alpha}}$ have significant variations and $C_{z\dot{\alpha}} < 0$ in the period of t= 7482.5 ~ 7491 sec in Fig. 5(b). It should be noted that $C_{z\dot{\alpha}}$ represents the virtual mass effect and is particularly large in transonic flow to affect the plunging motion [10]. The $(C_{zq})_{osc}$ and $(C_{mq})_{osc}$ are insufficient in oscillatory damping in the periods of t= 7484 ~ 7486 sec and t= 7490~ 7494 sec, as shown in Fig. 5(a). The effect of $\dot{\alpha}$ -derivative on $(C_{mq})_{osc}$ is to improve the stability in pitch in the periods of t= 7482.5 ~ 7484 sec and 7486~ 7488.5 sec. The magnitudes of $C_{l\dot{\beta}}$ in Fig. 5(d) and $(C_{lp})_{osc}$ in Fig. 5(c) are small; C_{lp} is not shown because it is small throughout. The values of $C_{n\dot{\beta}}$ are from positive at t= 7483 sec to negative at t= 7484 sec; $(C_{nr})_{osc}$ are from positive at t= 7483.5 sec to negative at t= 7485 sec. It implies that the effects of $\dot{\beta}$ -derivative is to cause the directional stability more unstable.

The $C_{z\dot{\alpha}}$ is in a nominal negative value and $C_{m\dot{\alpha}}$ is in a positive one in the period of t= 3928.5 ~ 3929.5 sec and then, $C_{z\dot{\alpha}}$ approaches to zero and $C_{m\dot{\alpha}}$ becomes negative value in the period of t= 3930 ~ 3931.5 sec, as shown in Fig. 6 (b). The effect of $\dot{\alpha}$ -derivative on $(C_{mq})_{osc}$ is to improve the stability in pitch after $t = 3929.5$ sec in Fig. 6(a). The magnitudes of $C_{l\dot{\beta}}$ and $(C_{lp})_{osc}$ are small in the period of t= 3928 ~ 3930.8 sec. The values of $C_{n\dot{\beta}}$ and $(C_{nr})_{osc}$ are positive in the period of t= 3928 ~ 3929 sec and then become negative in the period of t= 3929 ~ 3930.8 sec. It implies that the effects of $\dot{\beta}$ -derivative is to cause the directional stability more unstable.
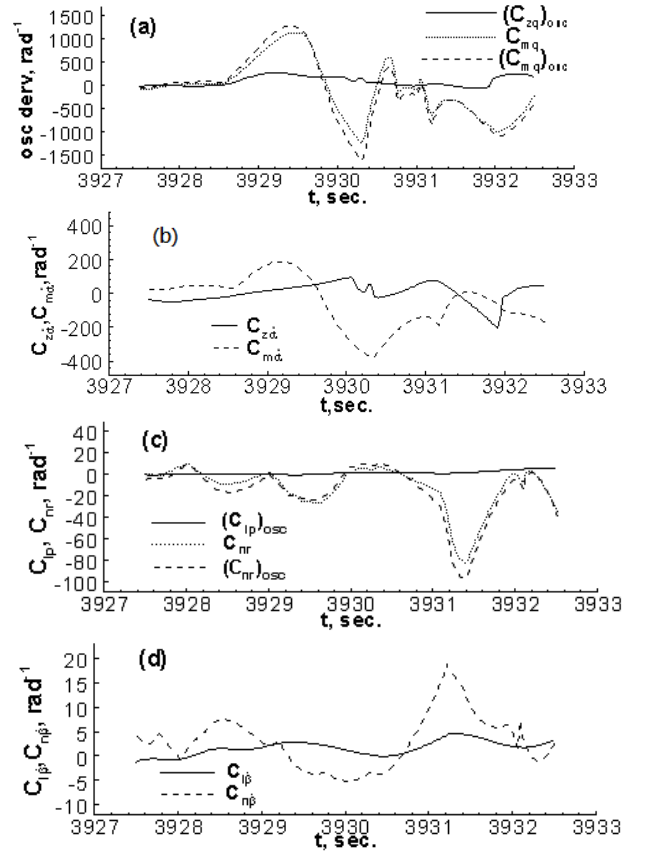

Fig. 6 Time history of main longitudinal and lateral-directional oscillatory derivatives for Transport B along the flight path

In essence, the effects of $\dot{\alpha}$ -derivative on $(C_{zq})_{osc}$, and $\dot{\beta}$ -derivative on $(C_{lp})_{osc}$ are small in Figs 5 and 6. However, the effect of $\dot{\alpha}$ -derivative on $(C_{mq})_{osc}$ is to improve the stability

in pitch; while the effects of $\dot{\beta}$-derivative is to cause more directional instability. These results indicate that the turbulent crosswind has some adverse effects on directional stability and damping. Although the dynamic derivatives tend to be small for the present two configurations, these are much helpful to understand the unknown factors of instability characteristics.

3.5 Eigenvalue Analysis of Flight Motion Modes

In the present study, the longitudinal and lateral-directional motion modes are analyzed based on the damping ratio (ζ) and undamped natural frequency (ω). The roots of the complex conjugate are as follows:

$$\lambda_{1,2} = -\zeta\omega_n \pm i\omega_n\sqrt{1-\zeta^2} \tag{15}$$

where $-\zeta\omega_n$ is real part (i.e. in-phase) and $\pm i\omega_n\sqrt{1-\zeta^2}$ are imaginary (i.e. out-of-phase) parts. λ_r and λ_i represent eigenvalues of real and imaginary parts, respectively. If λ_r is positive, the system is unstable; if it is negative, the system is stable [5].

Fig. 7 presents the eigenvalues of the short-period and phugoid modes for Transport A. The eigenvalues of real part in Fig. 7(a) are in small negative, except two portions at t= 7486.2 sec and t= 7492.0 ~7493.0 sec in small positive. The short period mode is typically a damped oscillation in pitch about the body y-axis in normal flight conditions. The short period mode is mostly in stable condition due to the value of $(C_{mq})_{osc}$ being mostly negative to have adequate pitch damping in oscillatory motions in the time span between t = 7484~7486 sec with largest drop-off height, as shown in Fig. 1(c), the highest a_z being 2.05g around t = 7483 sec and the lowest being -1.05 g around t = 7484 sec in Fig. 1(a), highest α about 4 deg. in Fig. 1(b). The eigenvalues of real part in Fig. 7(b) are positive and the magnitude varies like a mountain chain with pinnacle. The value of $(C_{zq})_{osc}$ is in negative and the magnitudes of $C_{z\dot{\alpha}}$ are also in negative values; $(C_{zq})_{osc}$ is insufficient in oscillatory damping and with virtual mass effects during sudden plunging motion to cause the phugoid mode in unstable condition. Note that part of the conventional phugoid mode has degenerated into

the plunging mode. Fig. 8 presents the eigenvalues of the Dutch roll, spiral, and roll modes. The eigenvalues of real part in Fig. 8(a) are positive in the time period of t= 4790~4794 sec. and all values in Fig. 8(b) are also positive, except the value of small portion at t= 7484 sec. The values of $(C_{nr})_{osc}$ are mostly positive; while $(C_{nr})_{osc}$ is insufficient in oscillatory damping to induce the unstable Dutch roll and spiral modes. The eigenvalues of real part in Fig. 8(c) are negative. The roll mode is stable because the values of $(C_{lp})_{osc}$ are mostly small negative to have some roll damping.
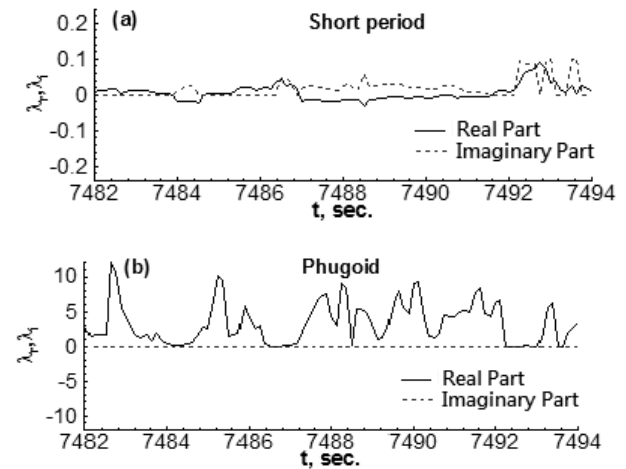

Fig. 7 Eigenvalues of longitudinal modes of motion for Transport A

Fig. 9 presents eigenvalues of longitudinal modes of motion for Transport B. The eigenvalues of real part in Fig. 9(a) are in negative, except two portions at t= 3828.8 sec and t= 3935.0 ~3938.0 sec in positive. The short period mode is mostly in stable condition due to the value of $(C_{mq})_{osc}$ is mostly negative to have adequate pitch damping in oscillatory motions in the time span between t = 3929.9~3930.5 sec with largest drop-off height, (around t = 3930 sec) as shown in Fig. 2(c). The eigenvalues of real part in Fig. 9(b) are positive at t= 3938.6~ 3929.8 sec. The value of $(C_{mq})_{osc}$ is positive and the magnitudes of $C_{m\dot{\alpha}}$ are also positive; $(C_{mq})_{osc}$ is insufficient in oscillatory damping during sudden plunging motion to cause the phugoid mode in unstable condition.

Fig. 10 presents the eigenvalues of the Dutch roll, spiral, and roll modes for Transport B. The eigenvalues of real part in Fig. 10(a) and

Fig. 10(b) are small positive in the time period of t= 3929.8~3933.0 sec. and t= 3931.2~3933.0 sec., respectively. The values of $(C_{nr})_{osc}$ are small positive at t=3929.8~3930.4 sec; while $(C_{nr})_{osc}$ is insufficient in oscillatory damping to induce the unstable Dutch roll and spiral modes. The eigenvalues of real part in Fig. 10(c) are negative, the roll mode is stable, except around t = 3930 sec..
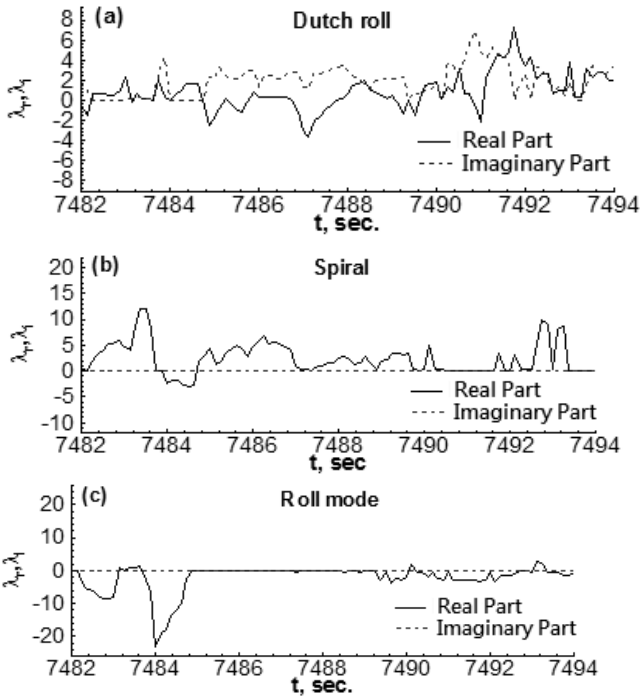

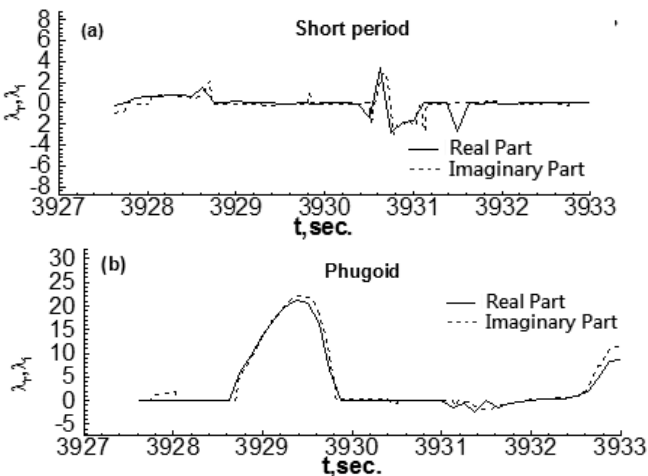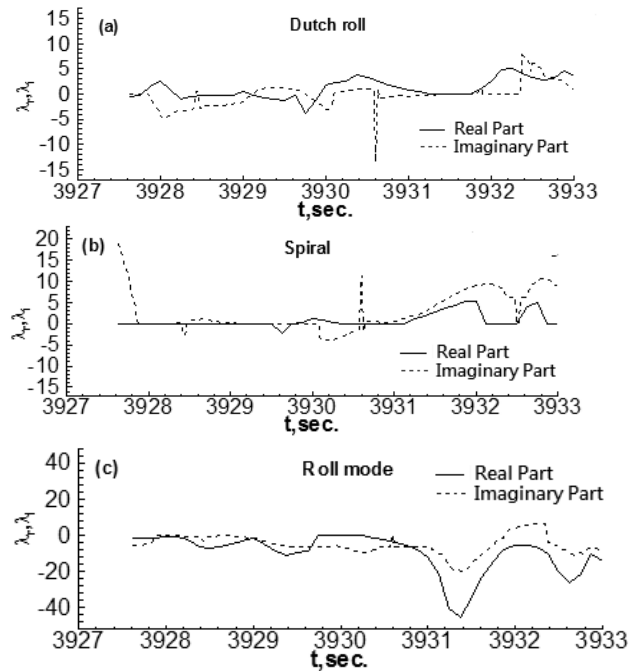Fig. 8 Eigenvalues of lateral-directional modes of motion for Transport A

Fig. 9 Eigenvalues of longitudinal modes of motion for Transport B

Fig. 10 Eigenvalues of lateral-directional modes of motion for Transport B

Airlines will not care too much about all the classical modes of motion. What they care about is the vertical plunging mode of motion which is not considered in the classical flight dynamics. According to [10], in vertical plunging motion the damping term is mainly related to $C_{z\dot{\alpha}}$. It may be possible to define the severity of plunging motion based on the vertical plunging equation of motion.

For the present purpose, if the severity is defined by the lowest load factor developed, then Transport A developed -1.05g with Δh=57.3m (around t = 7483 sec) and Transport B developed 0.02g with Δh=60m. Note that the phugoid mode of Transport A has positive real eigenvalues, but very small imaginary parts in phugoid (or plunging) mode (Fig. 7). However, the phugoid (or plunging) mode of Transport B is oscillatory with high frequency, but again with positive real eigenvalues. Small imaginary eigenvalues (or small frequency of the phugoid mode) imply small stiffness of the system. Therefore, it may be concluded that the plunging motion of Transport A is more severe because of its lower system stiffness. It should be noted that in the present FLM modeling, appropriate model-based filtering has been performed to filter out the high-frequency parts of the response so that the

characteristics of the plunging motion can be clearly exhibited.

4 Concluding Remarks

The main objective of this paper was to examine the flying qualities of a commercial transport aircraft in severe atmospheric turbulence with sudden plunging motion in transonic flight. The FLM technique was shown to be effective in establishing the nonlinear and unsteady aerodynamic models through the flight data of FDR. The aerodynamic models could generate oscillatory derivatives to examine the dynamic stability. The longitudinal and lateral-directional motion modes were analyzed through digital flight simulation based on decoupled dynamic equations of motion. The results of flight simulation showed that the Phugoid, Dutch roll, and spiral modes were in unstable conditions. Those unstable conditions were not only judged by the positive real part of the eigenvalues during sudden plunging motion, but also were due to insufficient oscillatory damping. Specifically, if severity of the plunging motion in affecting the flight safety is judged by the lowest load factor reached, then Transport A was worse than Transport B because it reached -1.05 g in the plunging motion as compared with 0.02g for Transport B. This was determined to be caused by low system stiffness in the plunging motion.

Acknowledgments

References

[1] Cornman, L.B., Morse, C., and Cunning, G., "Real-time estimation of atmospheric turbulence severity from in-situ aircraft measurements," *Journal of Aircraft*, Vol. 32, 1995, pp.171-177.

[2] Stewart, E. C., "Description of a Normal-Force In-Situ Turbulence Algorithm for Airplanes," NASA TM-2003-212666, Dec. 2003.

[3] Hamilton, D. W. and Proctor, F. H., "An Aircraft Encounter with Turbulence in the Vicinity of a Thunderstorm," AIAA Paper, 2003-4075, 2003.

[4] Chang, R. C., Ye, C. E., Lan, C. E., and Guan, W. L., " Stability Characteristics for Transport Aircraft Response to Clear-Air Turbulence," *Journal of Aerospace Engineering*, Vol. 23, No. 3, pp.197~204, July 2010.

[5] Chang, R. C., Ye, C. E., Lan, C. E., and Guan, W. L., "Flying Qualities for a Twin-Jet Transport in Severe Atmospheric Turbulence," *AIAA Journal of Aircraft*, Vol. 46, No. 5, Sept.-Oct. 2009.

[6] M. H. Yang, C. S. Ho, C. E. Lan, and F. B. Hsiao, "Longitudinal Handling Quality Analysis of a Civil Transport Aircraft Encountering Turbulence," *Journal of Aircraft*, Vol. 47, No. 1 (2010), pp. 32-40.

[7] Lan, C. E. and Chang, R. C. , *Chapter 7 Fuzzy-Logic Analysis of the FDR Data of a Transport Aircraft in Atmospheric Turbulence*, Part 2, Fuzzy Logic– Emerging Technologies and Applications, InTech – 51000, ISBN 978-953-51-0337-0, Rijeka, Croatia, March 16, 2012.

[8] Roskam, J*., Airplane Flight Dynamics and Automatic Flight Controls,* Part I*,* DAR Corporation, Lawrence, Kansas, 2003.

[9] Hovanessian. S. A. and Pipes, L. A., *Digital Computer Methods in Engineering*, McGraw-Hill Book Company, 1969.

[10] Sheu, D. and Lan, C. E., "Estimation of Turbulent Vertical Velocity from Nonlinear Simulations of Aircraft Response," *Journal of Aircraft*, Vol. 48, No. 2, March-April, 2011, pp.

Contact Author Email Address

Ray C. Chang.

E-mail address: raychang@cc.hc.cust.edu.tw

Copyright Statement